

A Kalman Filter-Based Algorithm for Simultaneous Time Synchronization and Localization in UWB Networks

Justin Cano, Saad Chidami and Jerome Le Ny

Abstract—The ability to accurately measure signal time-of-flight between ultra-wideband (UWB) wireless communication transceivers, even in multipath environments, makes this technology ideally suited to develop ranging-based positioning systems, especially for indoor applications where GPS signals are not available. In recent years, low-cost commercial UWB transceivers have become more easily available and increasingly used to develop custom robot positioning systems. In this paper, we focus in particular on positioning techniques requiring the synchronization of base stations such as Time of Arrival (TOA) and Time Difference of Arrival (TDOA). We present a protocol based on Kalman filtering for simultaneous synchronization of multiple UWB base stations and positioning of an arbitrary number of passive UWB receivers. We illustrate experimentally using our protocol and an EKF-based navigation system design the level of accuracy achievable with small low-power UWB modules for mobile robot positioning. We discuss in details measurement errors and system tuning issues applicable to popular commercial UWB transceivers.

I. INTRODUCTION

Maintaining an accurate location estimate, in real-time and by using only a small amount of computational and energy resources is crucial for any autonomous mobile robot. In view of their cost, accuracy, low power consumption, and increasing availability, Ultra-Wide Band (UWB) communication and positioning systems [1] are becoming a popular technology to develop robotic localization solutions based on ranging or angle-of-arrival measurements [2]–[8]. Various protocols exist to obtain distance measurements between radio-frequency transceivers using signal Time-of-Flight (ToF) measurements [1], [9], the main difficulty to overcome being the time measurement errors due to clock offsets at different nodes. These distance measurements can then be used to locate transceivers with unknown position (“tags”) in a network that includes enough nodes with known position (“anchors”).

Ranging protocols differ by their implementation complexity, the trade-off they offer between the speed and accuracy of individual ranging transactions, and the achievable measurement update frequency as the number of tags increases for a fixed number of anchors. Previous work on UWB-aided localization with a focus on robotic applications has used simple Two-Way Ranging protocols (TWR) [4], [8], which however can only support a limited number of tags, as well as more complex One-Way Ranging (OWR) protocols such

as Time of Arrival (TOA) and Time Difference of Arrival (TDOA), which scale to an arbitrary number of tags that moreover only operate as passive receivers, but require tight synchronization of the anchors [5]. The main focus of these papers is on the design of UWB-aided integrated navigation systems, e.g., based on Extended Kalman Filters (EKF) [9] to combine ranging and inertial sensor measurements. More detailed ranging measurement models for UWB systems, focusing in particular on non line of sight (NLOS) measurements, are discussed in [2], [3] for example. Such models are very beneficial to ultimately design higher performance and more reliable position estimators.

In this paper, we propose a protocol for simultaneous UWB anchor synchronization and OWR, supporting the localization of an arbitrary number of tags, and hence particularly appropriate for multi-robot systems. Moreover the tags act only as passive receivers, thereby reducing their energy consumption. The protocol, described in Section II-B, requires exchanging messages between the UWB anchors to synchronize them, while the tags use the emission and reception times of these synchronization messages to deduce ToF information and ultimately localize themselves. In contrast to some previous work such as [5], [10], our synchronization algorithm, described in Section III-A, relies on a dynamical model of the transceiver clock parameters (time and frequency offsets), which can therefore be time-varying and are estimated using a Kalman filter as in [11], [12]. Compared to [7], we do not discuss here *distributed* algorithms for joint anchor synchronization and localization, however the anchor synchronization accuracy we report is in the sub-ns level range, whereas the results in [7] show μs level accuracy, which is insufficient to support indoor localization services for the tags. Indeed, 1 μs error in a ToF measurement corresponds to a ranging error of $c \times 10^{-6} \approx 300$ m, where c is the speed of light. In addition, our Kalman filter-based synchronization scheme leverages frequency offset measurements provided by the phase recovery process of communicating UWB modules (see Section III) in addition to clock offset measurements obtained from timestamp differences. This feature seems to be rarely exploited in the literature.

An important contribution of this paper is to provide in Section III-D a methodology for the identification of the quantitative model necessary for the tuning of the synchronization Kalman filter. In Section IV, we then discuss experimental results obtained by integrating popular low-cost UWB transceivers (Decawave’s DW1000 [13]) into a custom embedded platform. Anchors are synchronized with

This work was supported in part by FRQNT under grant 2018-PR-253646 and CFQCU under grant 2018-FQ-211195. The authors are with department of Electrical Engineering, Polytechnique Montreal. J. Cano and J. Le Ny are also with GERAD, Montreal, QC H3T-1J4, Canada {justin.cano, saad.chidami, jerome.le-ny}@polymtl.ca.

sub-ns accuracy, and an extended Kalman filter (EKF) is presented to estimate the position of a mobile tag carried by a ground robot. This section serves to illustrate the practical performance achievable by UWB-based indoor localization systems, and some of the main sources of errors.

II. OVERVIEW OF TOF-BASED SYNCHRONIZATION, RANGING AND POSITIONING

A. System Description

Consider N anchors or base stations at fixed known positions $\mathbf{A}_i = [A_{i,x}, A_{i,y}, A_{i,z}]^T$, $0 \leq i \leq N-1$, in a global coordinate frame \mathcal{G} , each equipped with an UWB transceiver. Alongside the anchors, we have M tags E_j , $1 \leq j \leq M$, with *a priori* unknown positions $\mathbf{p}_j = [x_j, y_j, z_j]^T$, also equipped with UWB transceivers. For positioning applications, our goal is to estimate each \mathbf{p}_j in real-time. The tags can be mobile, in which case we write $\mathbf{p}_{j,k}$, $k \geq 0$, for the position of tag j at period k .

Any two nodes i, j in the network can exchange messages through their UWB modules. Node i can attempt to measure the ToF \tilde{t}_j^i of the messages exchanged with j and then deduce a *pseudo-range* measurement $\tilde{\rho}_j^i := c\tilde{t}_j^i$, which differs however from the true distance between these nodes because of ToF measurement errors and clock offsets between modules, as detailed in Section III. The pseudo-range measurements can then be used to localize the tags using Time-of-Arrival (TOA) or Time-Difference-of-Arrival (TDOA) schemes, relying on nonlinear least-squares or filtering techniques [1], [9], see Section IV for an example.

We describe next a protocol that can be used to synchronize the clocks of a limited number of anchors actively exchanging messages, and obtain ranging measurements between the anchors and an arbitrary number of tags operating as passive receivers. This protocol in fact does not use any knowledge of the position the anchors, so anchors and tags are only distinguished by the fact that they transmit messages or not. It turns out that anchors could at the same time play the role of tags to provide a self-localization service for the whole network, a more complicated scenario that we do not discuss here to simplify the exposition.

B. A Simultaneous Ranging and Synchronization Protocol

As mentioned in the introduction, the main source of error in pseudo-range measurements between two nodes comes from the offset between the internal clocks measuring time as these nodes. The simplest way to mitigate the effect of these clock offset errors is to employ TWR schemes between the nodes [1], [4], [14]. However, TWR protocols require the anchors to collect messages from each tag, which cannot scale to more than a few tags for applications requiring high accuracy and high position update frequencies. Alternatively, certain TOA and TDOA schemes work with tags that passively listen to messages broadcast by the anchors, and hence scale to an arbitrary number of tags [15]. However, these schemes typically require that the anchor clocks be synchronized, with a precision corresponding to the desired ranging accuracy, i.e., better than 1 ns to achieve

ranging measurement errors better than 30 cm. This in turn requires accurate clock model estimates and carefully designed protocols.

We describe our proposed protocol to simultaneously synchronize the anchors and obtain pseudo-range measurements between the anchors and the tags on Fig. 1. The clock of the anchor A_0 is chosen as the “master” clock, also denoted M , and indicates the chosen reference time of the system. The other anchors are called “slaves” and estimate at each instant the master’s time to correct their own clocks, by exchanging messages with M . Each tag E_j independently listens to these messages and attempts to deduce, from their timing and content, ToF measurements \tilde{t}_i^j from each anchor A_i in its range. For concreteness we include on Fig. 1 one master anchor, three slave anchors, and one tag.

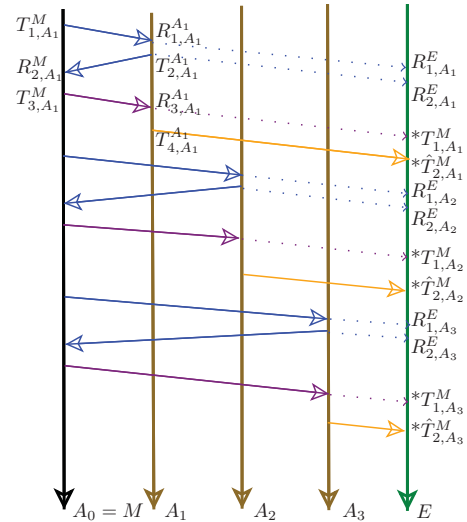


Fig. 1: Simultaneous ranging and synchronization protocol example with 4 anchors A_i , $i = 0, \dots, 3$ and one tag E .

Denote message transmission timestamps T_{l,A_i}^T and reception timestamps R_{l,A_i}^T , where A_i is a slave anchor, $l \in [1, 4]$ is a message number in a four-message transaction and τ denotes the clock measuring this timestamp. The timestamps preceded by an asterisk (*) are not measured by the UWB module but sent with the currently received message. Note that due to the wireless nature of the system, transmitted messages are received by all UWB nodes within range, allowing a given message to be used for different purposes by different receivers (anchor or tag).

The master M initiates a synchronization exchange periodically with each slave anchor A_i , $i \geq 1$, one after the other. It first sends a polling message ($l = 1$) and the slave replies with a response message ($l = 2$). The third message, sent by the master ($l = 3$), contains the values of the timestamps R_{2,A_i}^M and T_{1,A_i}^M measured by M . Note that in practice, an UWB module cannot send in a message the transmission timestamp of that same message. With its own timestamp measurements and those of M , the slave A_i estimates its clock offset, as detailed in Section III. A_i also broadcasts in a final message ($l = 4$) its estimate \hat{T}_{2,A_i}^M of the transmission

timestamp $T_{2,A_i}^{A_i}$ of the second message, with the clock offset correction to express it according to M 's time.

Consider now any tag E . By listening to the 4 messages exchanged by the master and the slave anchor i , it can obtain the transmission timestamp T_{1,A_i}^M and the synchronized estimate \hat{T}_{2,A_i}^M . It also measures the reception times R_{1,A_i}^E and R_{2,A_i}^E according to its own clock, and computes the following two *pseudo-ranges*

$$\begin{aligned}\tilde{\rho}_{A_0}^E &= c(R_{1,A_i}^E - T_{1,A_i}^M), \\ \tilde{\rho}_{A_i}^E &= c(R_{2,A_i}^E - \hat{T}_{2,A_i}^M),\end{aligned}\quad (1)$$

which can be related to the distances between the tag E at position \mathbf{p} and the anchor A_i at position \mathbf{A}_i by a model of the form

$$\tilde{\rho}_{A_i}^E = \|\mathbf{p} - \mathbf{A}_i\|_2 + c\delta_E + \nu_{A_i}^E, \quad (2)$$

where δ_E is the tag's clock offset with respect to the anchors' common time, and $\nu_{A_i}^E$ is some residual noise term. The pseudo-range measurements (1) can be used for tag localization (estimation of \mathbf{p}), as described in Section IV. In particular, a TOA system estimates δ_E for the tag at the same time as \mathbf{p} , whereas a TDOA system cancels the effect of δ_E by taking differences of pseudo-ranges $\tilde{\rho}_{A_i}^E - \tilde{\rho}_{A_j}^E$ for pairs of anchors. First, Section III details the clock offset estimation procedure, necessary to complete the description of the synchronization protocol.

III. ANCHOR SYNCHRONIZATION

Synchronization between the anchors is done by letting the slaves estimate their clock offset with respect to the master's clock. Sufficient accuracy (experimentally, sub-ns level on low-cost embedded systems) can be achieved by relying on a dynamical clock model and a Kalman filter, as described in this section. It is sufficient to focus here on two anchors, the master M and one slave anchor S to synchronize.

A. Clock Modeling and Synchronization

Time at each node in an UWB network is measured by the node's hardware clock, and in practice is provided to the software layer by incrementing a register at each period of a signal produced by a crystal oscillator [11], [16].

The oscillator's frequency varies in time around a nominal frequency, essentially because of thermodynamical effects [17]. Hence, two registers from two different clocks are not incremented at exactly the same rate, resulting in clock drift.

Let t^M and t^S denote the time as measured by M and S , respectively. Introduce the quantity δ called *clock offset*

$$\delta(t^S) := t^S - t^M(t^S), \quad (3)$$

which (from the point of view of S) is the difference between the time t^S measured by S and the time $t^M(t^S)$ measured by M at the exact same time t^S . Note that δ is time-varying in general. The time-derivative of δ is called the *skew*, and is precisely due to the instantaneous difference between the clock frequencies

$$\gamma(t^S) := \frac{d\delta(t^S)}{dt^S} = 1 - \frac{dt^M}{dt^S}. \quad (4)$$

Note that since dt^M/dt^S in (4) is close to one, γ remains relatively close to zero. The IEEE 802.15.4 standard [18] defines an UWB physical layer that specifies bounds of ± 40 ppm on the skew between two transceiver clocks.

To synchronize its timestamps with the master's time, the slave S needs an estimate $\hat{\delta}(t^S)$ of $\delta(t^S)$ at each time t^S . Then, from (3), the estimate $\hat{t}^M(t^S)$ by S of the time at the master is just

$$\hat{t}^M(t^S) = t^S - \hat{\delta}(t^S). \quad (5)$$

In practice, S obtains offset and skew estimates at discrete times t_k^S , $k \geq 0$, and can then form estimates of δ at any other time by the first order approximation

$$\hat{\delta}(t^S) \approx \hat{\delta}(t_k^S) + (t^S - t_k^S)\hat{\gamma}(t_k^S). \quad (6)$$

B. Available Measurements

Commercial UWB modules are designed to measure reception and emission timestamps relatively precisely. Some of them also output a "carrier integrator value", which provides a direct (noisy) measure $\tilde{\gamma}$ of the clock skew for two modules involved in a message transmission. The skew measurement is implemented in hardware and uses carrier recovery techniques [19], which rely on *a priori* known symbols in the preamble of each transmitted message [18].

Next, given the timestamps $T_{1,S}^M$, $R_{1,S}^S$, $T_{2,S}^S$, $R_{2,S}^M$ for a single synchronization exchange available at S as explained in Section II, a clock offset measurement can be formed as follows. From (3), we have

$$\delta(R_{1,S}^S) = R_{1,S}^S - t^M(R_{1,S}^S), \quad \delta(T_{2,S}^S) = T_{2,S}^S - t^M(T_{2,S}^S).$$

Moreover, assuming the ToF of the two messages $l = 1, 2$, is the same (ignoring in particular the motion of the tag or anchor during the exchange) and equal to t_a^M as measured according to M , we have

$$t^M(R_{1,S}^S) = T_{1,S}^M + t_a^M, \quad R_{2,S}^M = t^M(T_{2,S}^S) + t_a^M. \quad (7)$$

Eliminating $t^M(R_{1,S}^S)$, $t^M(T_{2,S}^S)$, we get

$$\begin{aligned}\tilde{\delta}(t_k^S) &\approx (\delta(R_{1,S}^S) + \delta(T_{2,S}^S))/2 \\ &= \frac{R_{1,S}^S - T_{1,S}^M - (R_{2,S}^M - T_{2,S}^S)}{2},\end{aligned}\quad (8)$$

where $t_k^S \approx (R_{1,S}^S + T_{2,S}^S)/2$. The computation (8) must be implemented carefully in practice because of timer wrapping with finite size clock registers. Since the approximation defining the measurement time t_k^S requires the duration of the exchange to be as small as possible [16], we chose based on our experiments to let the master communicate with each slave successively rather than parallelize the exchanges shown in blue on Fig. 1.

C. Clock Drift Dynamics and Estimator

Introduce $\mathbf{d} = [\delta \ \gamma]^T$ as the clock drift state vector. In continuous-time, we can consider the following stochastic second-order model for the dynamics for the drift

$$\dot{\mathbf{d}} = \mathbf{A}\mathbf{d} + \zeta := \begin{bmatrix} 0 & 1 \\ 0 & 0 \end{bmatrix} \mathbf{d} + \begin{bmatrix} \zeta_\delta \\ \zeta_\gamma \end{bmatrix}, \quad (9)$$

where ζ_δ and ζ_γ are uncorrelated zero-mean continuous white Gaussian noise processes with respective power spectral densities (PSD) $\sigma_{\delta\delta}^2$ and $\sigma_{\gamma\gamma}^2$. This model, assuming slow skew dynamics, is sufficiently precise for localisation purposes (see section IV) though [12] proposes a third-order offset tracking model. The discretization of (9) at times t_k^S , $k \geq 0$, with time-steps $h_k := t_k^S - t_{k-1}^S$, $k \geq 1$, leads to the following difference equation

$$\mathbf{d}_k = \begin{bmatrix} 1 & h_k \\ 0 & 1 \end{bmatrix} \mathbf{d}_{k-1} + \nu_k, \quad \text{with } \nu_k := \begin{bmatrix} \nu_{\delta,k} \\ \nu_{\gamma,k} \end{bmatrix} \sim \mathcal{N}(\mathbf{0}, \Sigma_k), \quad (10)$$

for $\mathbf{d}_k = [\delta_k \ \gamma_k]^T$, where [20]

$$\Sigma_k = \begin{bmatrix} \frac{h_k^3}{3} \sigma_{\gamma\gamma}^2 + h_k \sigma_{\delta\delta}^2 & \frac{h_k^2}{2} \sigma_{\gamma\gamma}^2 \\ \frac{h_k^2}{2} \sigma_{\gamma\gamma}^2 & h_k \sigma_{\gamma\gamma}^2 \end{bmatrix}. \quad (11)$$

We assume a discrete-time measurement model such that our measurements $\mathbf{y}_k = [\tilde{\delta}_k \ \tilde{\gamma}_k]$ of the clock offset and clock skew at times t_k^S are perturbed by zero-mean (discrete-time) white Gaussian noise $\omega_k := [\omega_{\delta,k}, \omega_{\gamma,k}]^T \sim \mathcal{N}(\mathbf{0}, \mathbf{R})$ as follows

$$\mathbf{y}_k = \mathbf{d}_k + \omega_k, \quad \text{with } \mathbf{R} = \begin{bmatrix} \sigma_{\delta m}^2 & 0 \\ 0 & \sigma_{\gamma m}^2 \end{bmatrix}. \quad (12)$$

We then implement a discrete-time Kalman Filter (KF) at each slave anchor S to produce a clock drift state estimate $\hat{\mathbf{d}}_k$ over time with respect to M . With the process dynamics (10) and measurement model (12), the standard Kalman filter equations are available in [21] for example.

D. Kalman Filter Tuning

The dynamic model of Section III-C requires careful tuning for the Kalman filter to achieve the necessary level of performance in synchronizing the clock of S . An overview of this tuning process is given in this section. First, the anchors M and S are placed at their desired positions, assumed favorable to unperturbed signal transmission along the direct path, i.e., they should be far from reflective surfaces, in direct line of sight, and the potential directivity of the antennas should be accounted for, see Section IV-A. We then collect a sufficiently large dataset of clock offset and skew measurements $\tilde{\delta}_k, \tilde{\gamma}_k$. The experimental data illustrating our discussion is obtained using the DW1000 UWB modules commercialized by the company Decawave [13].

1) *Measurement and Process Noise for the Skew:* After a warm-up phase for the clocks' crystals, a quasi-constant mean can be observed for the clock skew measurements over a period of about one hour, see Fig. 2. Assuming an approximately constant mean skew γ over a sample of L measurements, we can then estimate the skew measurement variance empirically by the formula

$$\sigma_{\gamma m}^2 \approx \frac{1}{L-1} \sum_{k=1}^L \left(\tilde{\gamma}_k - \frac{1}{L} \sum_{l=1}^L \tilde{\gamma}_l \right)^2 =: \text{empVar}(\tilde{\gamma}).$$

Next, to determine the process noise variance $\sigma_{\gamma\gamma}$, we proceed iteratively, using the whole dataset. Starting with an

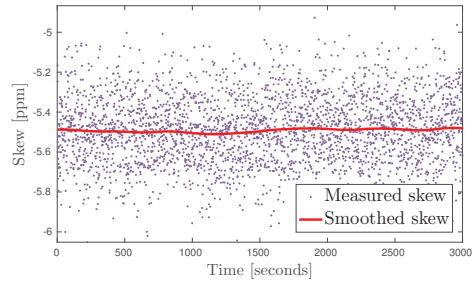


Fig. 2: Raw $\tilde{\gamma}$ measurement and smoothed value $\hat{\gamma}$.

TABLE I: Parameters for the synchronization KF.

$\sigma_{\delta\delta}$	$\sigma_{\delta m}$	$\sigma_{\gamma\gamma}$	$\sigma_{\gamma m}$
2.0×10^{-5}	1.58×10^{-10}	2.53×10^{-8}	1.69×10^{-7}

initial guess, we use a Rauch-Tung-Striebel smoother [22] to obtain an estimate $\hat{\gamma}_k$ of the skew sequence, see Fig. 2. We then compute a new value of $\sigma_{\gamma\gamma}$ from the empirical variance

$$\phi_k := \gamma_k - \gamma_{k-1} = \nu_{\gamma,k} \Rightarrow h_k \sigma_{\gamma\gamma}^2 \approx \text{empVar}(\phi). \quad (13)$$

We can then repeat this procedure until the value obtained for the empirical variance approximately agrees with the one used for the smoother.

2) *Measurement and Process Noise for the Clock Offset:* After setting the noise variances for the clock skew as above, we consider the parameters $\sigma_{\delta m}$ and $\sigma_{\gamma m}$. The measurement noise $\omega_{\delta,k}$ for the clock offset in the model is mainly due to timestamping errors at the hardware level. To select $\sigma_{\delta m}$, let ϵ be the residual synchronization error after Kalman filtering, so that $\hat{t}^M(R_{1,S}^S) = t^M(R_{1,S}^S) + \epsilon$. We have from (7) that

$$\epsilon = \hat{t}^M(R_{1,S}^S) - T_{1,S}^M - t_a^M = \hat{t}^M(R_{1,S}^S) - T_{1,S}^M - d/c,$$

where d is the distance between M and S . By measuring d , we there obtain a means of observing the residual synchronization errors, and the parameter $\sigma_{\delta m}$ can then be tuned to trade-off the steady-state variance of these errors with their convergence speed.

Finally, the noise ζ_δ and hence the parameter $\sigma_{\delta\delta}$ is mainly introduced to provide an additional parameter to adjust the transient behavior of these residual synchronization errors. As an indication, the values chosen for all parameters in our model, and hence for the Kalman filter implementation, are reported in Table I. Note that the tuning process is independent of the choice of the sampling intervals h_k , which in practice can be made of the order of a few milliseconds, but increases with the number of slave anchors to synchronize with M .

IV. IMPLEMENTATION AND RESULTS

In this section, we first discuss in more details the sources of error in ranging measurements obtained with UWB modules in indoor environments, which translate into positioning errors in subsequent algorithms. We then describe the impact

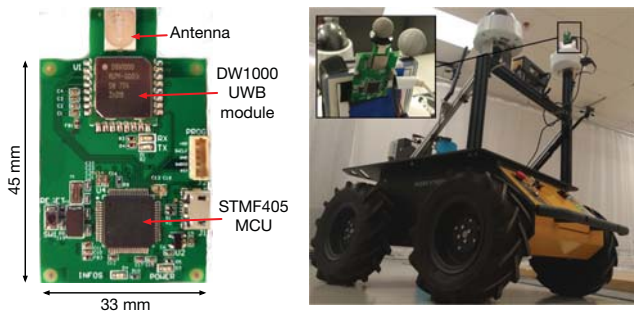


Fig. 3: Left: Our board with DWM1000 UWB module and microcontroller. Right: Husky UGV carrying an UWB tag.

of these errors on the accuracy of a navigation system for a mobile ground robot carrying an UWB tag. We implemented our synchronization algorithm on six anchors (1 master and 5 slaves). Anchors and tags in our system are implemented on the same hardware shown on the left of Fig. 3, a custom-designed board carrying a Cortex-M3 STM32F405 microcontroller connected to a DWM1000 module, the latter consisting of the DW1000 UWB chip [13] and an integrated omnidirectional antenna.

A. Ranging Measurement Errors

To characterize experimentally OWR measurement errors, we consider two anchors M and S with known distance d between them, and synchronize S to M as explained in Section III. Using either one of the expressions (7) together with the estimates (5) obtained from the synchronization filter, we deduce a ToF measurement \hat{t}_a between the two anchors. This corresponds to a ranging measurement $\hat{\rho}_S^M = c\hat{t}_a$, which differs from the true distance d because of measurement errors. Generalizing the simple error model (2), we can write

$$\hat{\rho}_S^M = d + \mu + b_{NLOS} + b_d + \nu_d,$$

where μ and b_{NLOS} are due to multipath interference and Non-Line-of-Sight (NLOS) measurements [23], b_d accounts for antenna directionality issues, and ν_d is a residual random error term, including anchor synchronization errors. These possible error terms are discussed in more details below.

1) *Multipath Interference and NLOS Measurements:* ToF measurements correspond to distance measurements between the UWB modules only when the reception time of the signal on the direct path, i.e., the signal traveling in straight line between the modules, is measured accurately. Especially for indoor environments, it is frequently the case that additional signals reflected by an obstacle, a wall, the ceiling or the ground, arrive at the receiver with considerable amplitude and create constructive or destructive interferences with the direct signal, called multipath interference [23]. This results in timestamp measurement errors μ at the receiver, which can be positive or negative.

UWB receivers are designed to provide some robustness against multipath interference [24]. However, sometimes the direct signal can also be severely attenuated or even blocked

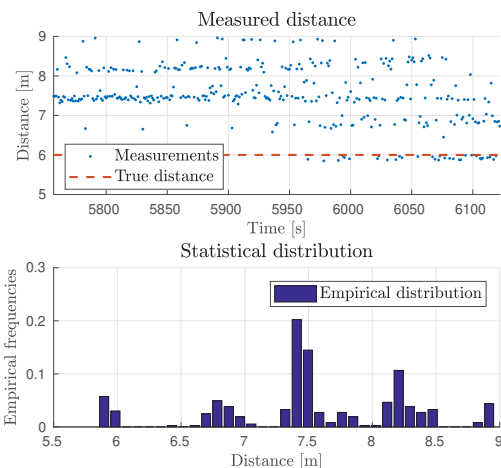


Fig. 4: Ranging measurements with significant NLOS errors for two UWB modules in proximity of a reflective ground surface.

by obstacles between the UWB modules. In such cases, receivers can lock onto reflected signals rather than the direct one and measure their timestamps, resulting in typically large positive errors in ToF and hence ranging measurements, see Fig 4. In a simple scheme, it is sometimes possible to detect NLOS measurements at the physical layer by monitoring the power level of the received signal [13] and then simply discard these measurements. Much work has been done however to detect and exploit NLOS measurements, see, e.g., [25]. At the application level, NLOS measurements can also be rejected by fault-detection techniques, see Section IV-B.

2) *Antenna Directionality Issues:* The relative angle between the UWB transmitter and receiver antennas can also impact ranging measurements. This phenomenon is due to the three dimensional radiation patterns of the antennas. In configurations where the received power is weak, the measurements of signal reception times become more noisy and typically delayed. In practice, this issue can be largely mitigated by avoiding these problematic configurations.

3) *Residual Random Errors:* Even after tuning our synchronization Kalman filter and placing the anchors in an environment favorable to ToF measurements, relatively small and transceiver specific errors remain. Any systematic measurement bias should be detected and compensated for, and could be due for example to signal propagation delays in the antenna. The remaining errors can then be considered random and approximately Gaussian, and can be due for example to the residual synchronization errors and to the limited accuracy with which the receiver can timestamp incoming signals [24].

B. An Example of UWB-Aided Navigation System

Finally, we illustrate the achievable performance and errors typically observed for an UWB-aided navigation system relying on our synchronization and ranging protocol for OWR. We designed system based on an extended Kalman

filter (EKF) [9] and TOA to estimate the position $\mathbf{p} = [x, y, z]$ and velocity $\mathbf{v} = [v_x, v_y, v_z]$ of a mobile UWB tag. For a TOA scheme, the tag also estimates the drift δ, γ of its clock with respect to the anchors' time. Hence, let $\mathbf{x} = [x \ v_x \ y \ v_y \ z \ v_z \ \delta \ \gamma]^T$ be the state vector to estimate. We assume here a simple 3D kinematic model for the state dynamics

$$\dot{\mathbf{x}} = \mathbf{L}\mathbf{x} + \mathbf{G}\xi, \quad \text{with } \mathbf{L} = \mathbf{I}_4 \otimes \begin{bmatrix} 0 & 1 \\ 0 & 0 \end{bmatrix}, \quad (14)$$

where \otimes denotes the Kronecker product, the vector $\xi = [\xi_{v_x} \ \xi_{v_y} \ \xi_{v_z} \ \nu_\delta \ \nu_\gamma]^T$ is a noise term, and

$$\mathbf{G} = \begin{bmatrix} \mathbf{G}_\xi & \mathbf{0}_{6 \times 2} \\ \mathbf{0}_{2 \times 3} & \mathbf{I}_2 \end{bmatrix} \quad \text{with } \mathbf{G}_\xi = \mathbf{I}_3 \otimes \begin{bmatrix} 0 \\ 1 \end{bmatrix}.$$

The process ξ is assumed to be a continuous-time Gaussian white noise with diagonal PSD matrix $\Xi = \text{diag}(\sigma_{v_x}^2, \sigma_{v_y}^2, \sigma_{v_z}^2, \sigma_{\delta\delta}^2, \sigma_{\gamma\gamma}^2)$. Note that the tag's clock is similar to the clocks carried by the anchors, so the dynamics of δ, γ is the same as (9). We can then discretize (14) with the time steps h_k to obtain the discrete-time model

$$\mathbf{x}_k = \mathbf{A}\mathbf{x}_{k-1} + \xi_k, \quad (15)$$

with $\mathbf{A} = e^{\mathbf{L}h_k} = \mathbf{I}_8 + \mathbf{L}h_k$ and $\xi_k \sim \mathcal{N}(\mathbf{0}, \mathbf{Q}_k)$. The process noise covariance matrix is $\mathbf{Q}_k = \int_0^{h_k} e^{\mathbf{L}t} \mathbf{G}\Xi\mathbf{G}^T e^{\mathbf{L}^T t} dt$, which gives

$$\mathbf{Q}_k = \text{diag}(\mathbf{H}_k \sigma_{v_x}^2, \mathbf{H}_k \sigma_{v_y}^2, \mathbf{H}_k \sigma_{v_z}^2, \Sigma_k),$$

for $\mathbf{H}_k = \begin{bmatrix} \frac{h_k^3}{2} & \frac{h_k^2}{2} \\ \frac{3}{2} h_k^2 & h_k \end{bmatrix}$ and Σ_k given in (11). For every

message exchange in our protocol between $A_0 = M$ and anchor A_i for $i \geq 1$, the tag collects two pseudo-range measurements (1), one for M and one for A_i . Assuming that NLOS errors are negligible, the measurement model for these pseudo-range measurements is given by (2), where $\nu_{A_i}^E$ can be assumed to be Gaussian. These (nonlinear) measurements are combined with the dynamic model (15) through an EKF to provide an estimate $\hat{\mathbf{x}}$ of the state \mathbf{x} . This requires, for the EKF measurement update step [20], the linearization of the measurement model (2) at the current estimate $\hat{\mathbf{x}}$

$$\left. \frac{\partial \tilde{\rho}_{A_i}^E}{\partial \mathbf{x}} \right|_{\hat{\mathbf{x}}} = \begin{bmatrix} \frac{\hat{x} - A_{i,x}}{\|\hat{\mathbf{p}} - \mathbf{A}_i\|} & 0 & \frac{\hat{y} - A_{i,y}}{\|\hat{\mathbf{p}} - \mathbf{A}_i\|} & 0 & \frac{\hat{z} - A_{i,z}}{\|\hat{\mathbf{p}} - \mathbf{A}_i\|} & 0 & c & 0 \end{bmatrix}.$$

In practice, measurements contaminated by NLOS measurement errors are rejected in the EKF measurement update step by a simple test detecting large residuals $\hat{\rho}_{A_i}^E - \tilde{\rho}_{A_i}^E$, i.e., the difference between the expected and actual pseudo-range measurements [9].

1) *Experimental results:* The EKF performance was tested in 2D for an UWB tag carried on a mast by a Husky Unmanned Ground Vehicle (UGV), as shown on the right of Fig. 3. The accuracy of the state estimates $\hat{\mathbf{p}}, \hat{\mathbf{v}}$ can be evaluated by comparison to the reference measurements $\mathbf{p}_{ref}, \mathbf{v}_{ref}$ obtained with a motion capture system with a standard positioning error of 0.5 mm, serving as ground truth. Note that the EKF above is based on a generic kinematic

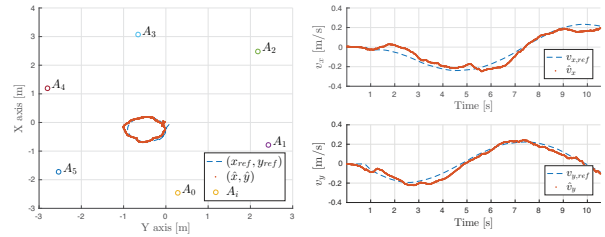


Fig. 5: Reference and estimated tag positions and velocities.

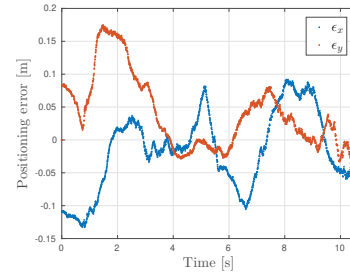


Fig. 6: Errors in the position estimates.

model and does not exploit the nonholonomic constraints on the UGV's trajectory.

Fig. 5 shows an example of trajectory and velocity estimates obtained for a small circular trajectory performed inside the convex hull of the six anchors. The positioning accuracy of the estimator for this trajectory can be more easily quantified using the error plot of Fig. 6, where $\epsilon = \hat{\mathbf{p}} - \mathbf{p}_{ref}$. The typical average positioning error is of the order of 8 cm, with a $2.5 \times 10^{-3} m^2$ variance. The achieved update rate is slightly superior 200 Hz, i.e., we obtain approximately every 5 ms two pseudo-range measurements (1), one for the master anchor and the other one for one of the slave anchors. A video available in the supplementary materials describes an additional experiment on a more complex trajectory that illustrates the effect of NLOS errors.

V. CONCLUSIONS

We present a protocol and Kalman filter-based algorithm for simultaneous synchronization and ranging in UWB networks. The protocol supports the design of hybrid networks combining anchors with synchronized clocks actively exchanging messages, and tags acting passive receivers that can deduce ranging information between themselves and the anchors by listening to these messages. The synchronization performance attained in practice is below 1 ns and the corresponding ranging accuracy below 20 cm in favorable environments. We also discussed how larger measurement errors can occur, in particular due to NLOS measurements. Finally, a basic example of an EKF-based navigation system was discussed to illustrate how the ranging measurements can be exploited for robot positioning applications.

ACKNOWLEDGMENT

The authors thank Wassim Rafrafi for his help at the beginning of this project.

REFERENCES

- [1] Z. Sahinoglu, S. Gezici, and I. Guvenc, *Ultra-wideband Positioning Systems: Theoretical Limits, Ranging Algorithms, and Protocols*. Cambridge University Press, 2008.
- [2] A. Prorok, L. Gonon, and A. Martinoli, "Online model estimation of ultra-wideband TDOA measurements for mobile robot localization," in *Proceedings of the IEEE International Conference on Robotics and Automation (ICRA)*, May 2012.
- [3] A. Prorok, "Models and algorithms for ultra-wideband localization in single- and multi-robot systems," Ph.D. dissertation, Ecole Polytechnique Fédérale de Lausanne (EPFL), 2013.
- [4] M. W. Mueller, M. Hamer, and R. D'Andrea, "Fusing ultra-wideband range measurements with accelerometers and rate gyroscopes for quadcopter state estimation," *Proceedings of the IEEE International Conference on Robotics and Automation (ICRA)*, May 2015.
- [5] A. Ledergerber, M. Hamer, and R. D'Andrea, "A robot self-localization system using one-way ultra-wideband communication," in *Proceedings of the IEEE/RSJ International Conference on Intelligent Robots and Systems (IROS)*. IEEE, 2015.
- [6] R. Zandian and U. Witkowski, "Robot self-localization in ultra-wideband large scale multi-node setups," *Proceedings of the 14th Workshop on Positioning, Navigation and Communications (WPNC)*, Oct 2017.
- [7] A. Alanwar, H. Ferraz, K. Hsieh, R. Thazhath, P. Martin, J. Hespanha, and M. Srivastava, "D-SLATS: Distributed simultaneous localization and time synchronization," in *Proceedings of the 18th ACM International Symposium on Mobile Ad Hoc Networking and Computing*, Jul 2017.
- [8] V. Mai, M. Kamel, M. Krebs, A. Schaffner, D. Meier, L. Paull, , and R. Siegwart, "Local positioning system using UWB range measurements for an unmanned blimp," *IEEE Robotics and Automation Letters*, vol. 3, no. 4, pp. 2971–2978, October 2018.
- [9] P. D. Groves, *Principles of GNSS, inertial, and multisensor integrated navigation systems*, 2nd ed. Artech House, 2013.
- [10] R. T. Rajan and A. J. van der Veen, "Joint ranging and synchronization for an anchorless network of mobile nodes," *IEEE Transactions on Signal Processing*, vol. 63, no. 8, pp. 1925–1940, April 2015.
- [11] G. Giorgi and C. Narduzzi, "Performance analysis of Kalman-filter-based clock synchronization in IEEE 1588 networks," *IEEE Transactions on Instrumentation and Measurement*, vol. 60, no. 8, pp. 2902–2909, August 2011.
- [12] M. Hamer and R. D'Andrea, "Self-Calibrating Ultra-Wideband Network Supporting Multi-Robot Localization," *IEEE Access*, vol. 6, pp. 22 292–22 304, 2018.
- [13] Decawave, *DW1000 Datasheet and user manual*, Decawave LTD, 2017, v2.12.
- [14] D. Neiryneck, E. Luk, and M. McLaughlin, "An alternative double-sided two-way ranging method," in *Proceedings of the 13th Workshop on Positioning, Navigation and Communications (WPNC)*, October 2016.
- [15] G. E. Garcia, L. S. Muppirisetty, E. M. Schiller, and H. Wymeersch, "On the Trade-Off Between Accuracy and Delay in Cooperative UWB Localization: Performance Bounds and Scaling Laws," *IEEE Transactions on Wireless Communications*, vol. 13, no. 8, pp. 4574–4585, Aug. 2014.
- [16] B. R. Hamilton, X. Ma, Q. Zhao, and J. Xu, "ACES: adaptive clock estimation and synchronization using Kalman filtering," in *Proceedings of the 14th ACM International Conference on Mobile Computing and Networking*, 2008.
- [17] M. Frerking, *Crystal Oscillator Design and Temperature Compensation*. Springer, 1978.
- [18] "802.15.4-2015 - IEEE standard for low-rate wireless networks." [Online]. Available: <https://ieeexplore.ieee.org/document/7460875/>
- [19] K. Aldubaikhy, "Differential code-shifted reference impulse-radio ultra-wideband receiver: Timing recovery and digital implementation," Master's thesis, Dalhousie University, Aug 2012.
- [20] Y. Bar-Shalom, X. R. Li, and T. Kirubarajan, *Estimation with applications to tracking and navigation: theory, algorithms and software*. John Wiley & Sons, 2004.
- [21] C. K. Chui and G. Chen, *Kalman Filtering with Real Time Applications*, 4th ed. Springer, 1987.
- [22] H. E. Rauch, C. T. Striebel, and F. Tung, "Maximum likelihood estimates of linear dynamic systems," *AIAA Journal*, vol. 3, no. 8, pp. 1445–1450, August 1965.
- [23] P. D. Groves, Z. Jiang, M. Rudi, and P. Strode, "A portfolio approach to NLOS and multipath mitigation in dense urban areas," in *Proceedings of ION-GNSS+*, September 2013.
- [24] A. Bensusky, *Wireless positioning technologies and applications*, 2nd ed. Artech House, 2016.
- [25] S. Venkatesh and R. M. Buehrer, "NLOS mitigation using linear programming in ultrawideband location-aware networks," *IEEE Transactions on Vehicular Technology*, vol. 56, no. 5, pp. 3182–3198, 2007.